JAERI-M
93-187

CREEP-FATIGUE INTERACTION PROPERTY OF A NICKEL-BASE HEAT-RESISTANT ALLOY HASTELLOY XR IN SIMULATED HTGR HELIUM GAS ENVIRONMENT

October 1993

Hirokazu TSUJI and Hajime NAKAJIMA

日本原子力研究所
Japan Atomic Energy Research Institute

JAERI-Mレポートは，日本原子力研究所が不定期に公刊している研究報告書です。
入手の問合わせは，日本原子力研究所技術情報部情報資料課（〒319-11茨城県那珂郡東海村）あて，お申しこしください。なお，このほかに財団法人原子力弘済会資料センター（〒319-11 茨城県那珂郡東海村日本原子力研究所内）で複写による実費頒布をおこなっております。

JAERI-M reports are issued irregularly.
Inquiries about availability of the reports should be addressed to Information Division, Department of Technical Information, Japan Atomic Energy Research Institute, Tokai-mura, Naka-gun, Ibaraki-ken 319-11, Japan.

編集兼発行　日本原子力研究所
印　　刷　㈱原子力資料サービス

JAERI-M 93-187

Creep-fatigue Interaction Property of a Nickel-base Heat-resistant Alloy Hastelloy XR in Simulated HTGR Helium Gas Environment

Hirokazu TSUJI and Hajime NAKAJIMA

Department of Materials Science and Engineering
Tokai Research Establishment
Japan Atomic Energy Research Institute
Tokai-mura, Naka-gun, Ibaraki-ken

(Received September 1, 1993)

The properties of Hastelloy XR, which is a developed alloy as the structural material for high-temperature components of the HTTR, under creep-fatigue interaction conditions were examined by performing a series of axial strain controlled fully reversed fatigue tests in the simulated HTGR helium gas environment at 700, 800, 900 and 950°C. Two types of evaluation techniques, i.e., the life fraction rule and the ductility exhaustion one, were applied for the evaluation of the creep damage during the tensile strain holding.

The fatigue life reduction due to the strain holding is observed even at hold times of 6 seconds, and the saturation point of the fatigue life reduction shifts to the shorter hold time side with increasing temperature. The life fraction rule predicts an excessively conservative value for the creep damage. The ductility exhaustion rule can predict the fatigue life under the effective creep condition much more successfully than the life fraction one.

Keywords: HTGR, Nickel-base Alloy, Heat-resistant Alloy, Hastelloy XR, Helium Coolant, High-temperature Low-cycle Fatigue, Creep-fatigue Interaction, Hold Time Effect, Life Fraction Rule, Ductility Exhaustion Rule

JAERI-M 93-187

高温ガス炉模擬ヘリウムガス雰囲気中における ニッケル基耐熱合金ハステロイ XR のクリープ・疲労特性

日本原子力研究所東海研究所材料研究部
辻　宏和・中島　甫

（1993年9月1日受理）

高温工学試験研究炉の高温構造用部材として開発したハステロイ XR を供試材料として，一連の軸ひずみ制御高温低サイクル疲労試験を700～950℃域の高温ガス炉1次冷却材模擬ヘリウムガス中で行い，この合金のクリープ・疲労特性を調べた。ひずみ波形は，三角波及び引張り側最大ひずみ時に保持を伴う台形波とした。ひずみ保持中のクリープ損傷を累積損傷和則と延性消耗則で評価した。引張り側に，わずか6秒のひずみ保持を与えた場合でさえ疲労寿命の低下が生じた。また，高温ほどひずみ保持導入に伴う疲労寿命低下の飽和が短時間側に移行した。累積損傷和則によるクリープ損傷評価は過度に安全側の寿命予測を与えるのに対して，延性消耗則によるクリープ損傷評価は寿命予測精度が優れていた。

東海研究所：〒319－11　茨城県那珂郡東海村白方字白根2－4

Contents

目　　次

1. Introduction

In the course of Japanese research and development of high-temperature gas-cooled reactors (HTGRs), the High-Temperature Engineering Test Reactor (HTTR) was planned to be constructed as the first reactor, and it is currently under construction at Oarai Research Establishment of the Japan Atomic Energy Research Institute. A nickel-base heat-resistant alloy, Hastelloy XR was developed as the structural material for high-temperature components of the HTTR [1-3]. Hastelloy XR has the common basal composition for the major constituents with Hastelloy X (i.e., nominally Ni - 22 mass% Cr - 18 mass% Fe - 9 mass% Mo), while minor elements such as Mn and Si are adjusted in the optimum ranges and Al, Ti and Co are eliminated to the lowest possible levels [1,3]. As the result of the above-mentioned modification, Hastelloy XR is known to have the substantially improved corrosion resistance in the simulated HTGR helium gas environment and the improved applicability to the HTTR relative to Hastelloy X [1-3].

The components of HTGRs are exposed to cyclic loadings, which arise during start-up and shut-down or power transients, at high temperatures. It is necessary, therefore, to examine the properties of the structural material under creep-fatigue interaction conditions for the design and safety evaluation of the high-temperature components. In the present study, the properties of Hastelloy XR under such conditions were examined by performing a series of axial strain controlled fully reversed fatigue tests in the impure helium environment simulating the primary coolant of HTGRs. Two types of evaluation techniques, i.e., the life fraction rule [4,5] and the ductility exhaustion rule [6-8], were applied for the evaluation of the creep damage during the strain holding.

2. Experimental Procedures

2.1 Material

The material tested in this study is Hastelloy XR bar commercially manufactured. The chemical composition and the tensile properties of the material are listed in Tables 1 and 2, respectively. The material was prepared by hot forging followed by solution annealing at 1200°C for 1 hour and water quenching.

2.2 Low-cycle Fatigue Tests

Low-cycle fatigue tests were accomplished using the specimens with 10 mm in diameter, 20 mm in length of the parallel portion and 15 mm in gauge length. The geometry of the specimen used in this study is shown in Fig. 1. Some tests were performed with a computer-controlled electro-hydraulic testing machine, and others were done with a computer-controlled electro-mechanical testing machine. The dynamic loading capacity of the both machines was 50 kN. The test section of the each machine was encased in an ultra-high vacuum tight chamber connected to a circulating helium loop system. The specimen was heated by induction heating. A series of axial strain controlled fully reversed fatigue tests was conducted at 700, 800, 900 and 950°C in the simulated HTGR helium gas environment. The impurity contents in the gas is indicated in Table 3. The characterization of the environment has been reported elsewhere [9].

Two types of strain waveforms were employed, i.e., a symmetric triangular waveform and a trapezoidal one with hold times of 6, 60, 600 and 3600 seconds. A strain rate of 0.1 %/s was applied in every test. The hold times were always introduced at a maximum tensile strain, because this type of hold-time experiments showed shorter fatigue life than compressive or symmetrical hold-time experiments in the previous studies [10,11].

3. Results and Discussion

3.1 Low-cycle Fatigue Properties

Table 4 summarizes the result of low-cycle fatigue tests with the symmetric triangular strain waveform. Figure 2 shows the relation between the total strain range and the number of cycles to failure obtained with the symmetric triangular strain waveform. The relation between them can be expressed as the sum of two simple power law terms for the elastic and the inelastic components of the total strain range as follows;

$$\Delta\varepsilon_t = 1.140\ N_f^{-0.122} + 24.157\ N_f^{-0.560} \quad \text{at } 700°C, \quad (1)$$

$$\Delta\varepsilon_t = 0.791\ N_f^{-0.117} + 59.191\ N_f^{-0.644} \quad \text{at } 800°C, \quad (2)$$

$$\Delta\varepsilon_t = 0.282\ N_f^{-0.0296} + 70.320\ N_f^{-0.689} \quad \text{at } 900°C, \quad (3)$$

$$\text{and } \Delta\varepsilon_t = 0.263\ N_f^{-0.0379} + 50.139\ N_f^{-0.637} \quad \text{at } 950°C, \quad (4)$$

where $\Delta\varepsilon_t$ is the total strain range in percent and N_f is the number of cycles to failure. In the present study N_f is determined as the number of cycles at which the maximum stress level is equivalent to 75 % of the maximum stress level in the stable stage or to 75 % of the extrapolated trend line of the maximum stress level according to the Japanese Industrial Standards Z 2279 [12].

Table 5 summarizes the result of low-cycle fatigue tests with the trapezoidal strain waveform. Figure 3 shows the relation between the fatigue life and the strain hold time with the trapezoidal strain waveform. The fatigue life reduction due to the holding is observed even at hold times of 6 seconds, and it becomes steeper with increasing temperature. It is noticed that the saturation point of the fatigue life reduction shifts to the shorter hold time side with increasing temperature. The trend is consistent with the fact that a much rapider drop of the stress occurs in the first few seconds during the strain holding at 900 and 950°C than that at 700°C.

3.2 Creep Properties for Creep Damage Evaluation

The creep properties of the same heat material as that in the present study have already been obtained in a simulated HTGR helium environment in other studies [13,14] by the authors. Although the impurity content levels in the gas were a little bit different from those in the present study, the characterizations of the both environments are essentially equivalent from the viewpoints of the chemical reactions between the material and the environment [9]. The data, therefore, were utilized for the evaluation of creep damage during the strain hold. The data on the creep properties were expressed with the Larson-Miller parameter [15], which is one of the most well known time-temperature parameters, in the present study.

Figure 4 shows the relation between the applied stress and the Larson-Miller parameter. The relation between them can be expressed as follows;

$$T(14.4+\log_{10}t_R) = 25795.5-1824.21\ \log_{10}\sigma-1142.98(\log_{10}\sigma)^2, \qquad (5)$$

where "T" is the temperature in Kelvin, t_R is the time to rupture in hour and σ is the applied stress in MPa.

Figures 5 and 6 show the relation between the applied stress and the Larson-Miller type parameter concerning the strain at rupture and the minimum creep rate, respectively. As can be seen in the figures, these properties are also successfully expressed with the Larson-Miller type parameter. Tensile properties given in Table 2 are also indicated in Figs. 5 and 6 as solid symbols. The relation between the stress and the Larson-Miller type parameter can be expressed as follows;

$$T(-4.5+\log_{10}\varepsilon_R) = -4797.52+264.684\ \log_{10}\sigma+306.946(\log_{10}\sigma)^2, \qquad (6)$$

$$T(-20.6+\log_{10}\dot{\varepsilon}_{min}) = -36172.9+5607.28\ \log_{10}\sigma+498.884(\log_{10}\sigma)^2, \qquad (7)$$

where "T" is the temperature in Kelvin, ε_R is the strain at rupture in percent, $\dot{\varepsilon}_{min}$ is the minimum creep rate or the strain rate for creep or tensile data in %/h and σ is the applied stress or the ultimate tensile

strength for creep or tensile data in MPa, respectively. In eqs. (5) through (7), the constants in the parameters and the coefficients in the regression equations were determined to provide the best fit to the creep data. The critical stress level, below which eq. (6) could be applied and above which the strain at rupture was assumed to be constant, was determined at each temperature as shown in Fig. 4.

The creep properties indicated in Figs. 4 through 6 were utilized for the evaluation of the creep damage during the strain holding in the present study.

3.3 Damage Evaluation Method

The fatigue damage in the test results with the trapezoidal strain waveform was evaluated as follows based on the concept proposed by Miner [16].

$$D_f = \frac{n}{N_f} , \tag{8}$$

where D_f is the fatigue damage, "n" is the number of cycles to failure observed with the trapezoidal strain waveform and N_f is the number of cycles to failure calculated with eqs. (1) through (4) in the same total strain range and temperature condition of the symmetric triangular waveform.

The stress level during the strain holding was measured continuously and stored into the computer at intervals of 0.05 second, which was applied in the earliest stage from the beginning of the strain holding, to 20 seconds, which were applied in the latest stage of the long period strain hold tests, in the experiments with a trapezoidal strain waveform. The stress level was assumed to be constant between the contiguous two measured points, and to be equal to the mean value of them as illustrated in Fig. 7 in the creep damage evaluation for convenience sake. The creep damage during the strain holding per cycle was evaluated using the measured stress data at the half cycle of the fatigue life.

Applying the life fraction rule [4,5], the creep damage during the strain holding was evaluated as follows.

$$D_{cl} = \sum_i \frac{\Delta t_i}{t_{Ri}} \times n \ , \qquad (9)$$

where D_{cl} is the creep damage by the life fraction rule, Δt_i is the period of time spent under a particular temperature and stress, which is a measured value during the strain holding at the half cycle of the fatigue life, t_{Ri} is the rupture time, which is calculated with eq. (5), corresponding to this temperature and stress, and "n" is the number of cycles to failure observed with the trapezoidal strain waveform.

Applying the ductility exhaustion rule [6-8], the creep damage during the strain holding was evaluated as follows in the present study.

$$D_{cd} = \sum_i \frac{\dot{\varepsilon}_{min} \Delta t_i}{\varepsilon_{Ri}} \times n \ , \qquad (10)$$

where D_{cd} is the creep damage by the ductility exhaustion rule, Δt_i is the period of time spent under a particular temperature and stress, which is a measured value during the strain holding at the half cycle of the fatigue life, $\dot{\varepsilon}_{min}$ is the minimum creep rate, which is calculated with eq. (7), corresponding to this temperature and stress, and ε_{Ri} is the strain at rupture, which is calculated with eq. (6), corresponding to this temperature and stress, and "n" is the number of cycles to failure observed with the trapezoidal strain waveform.

3.4 Results of Damage Evaluation

Table 6 summarizes the results of damage evaluation in the above-mentioned method. Figures 8 and 9 show the D_f versus D_{cl} plots and the D_f versus D_{cd} plots, respectively. The data are generally located in the higher portion than the line which shows the summation of the fatigue damage and the creep one is equal to unity in Fig. 8, i.e., in the life fraction rule. On the other hand, the data are lying near the line which shows the summation of the fatigue damage and the creep one is equal to

unity in Fig. 9, i.e., in the ductility exhaustion rule.

Assuming that the failure will occur when the summation of the fatigue damage and the creep one is equal to unity, the number of cycles to failure was predicted. The relations between the experimental and the predicted values by the life fraction rule and by the ductility exhaustion one are indicated in Figs. 10 and 11, respectively. In the figures, figures indicate the strain hold time in seconds. The trend is observed that the experimental fatigue life becomes shorter than the predicted one with increasing the strain hold time in these figures. As can be seen in Fig. 10, which corresponds to the life prediction method proposed by Taira [17], the data are generally located in the higher portion than the line which shows both the experimental and the predicted values are equal, i.e., the life fraction rule predicts an excessively conservative value for the creep damage. On the contrary, both the experimental and the predicted values agree well in Fig. 11. Comparison of Fig. 11 with Fig. 10 clearly shows that the ductility exhaustion rule can predict the fatigue life of Hastelloy XR under the effective creep condition much more successfully than the life fraction one though the reliability of the high temperature components may be ensured by limiting the summation of the fatigue damage and the creep one by the life fraction rule within unity. In Fig. 10 the trend is also observed that the life fraction rule may successfully predict the fatigue life under the longer strain holding conditions.

4. Conclusions

The properties of Hastelloy XR under creep-fatigue interaction conditions were examined by performing a series of axial strain controlled fully reversed fatigue tests in the simulated HTGR helium gas environment at 700, 800, 900 and 950°C. Two types of evaluation techniques, i.e., the life fraction rule and the ductility exhaustion one, were applied for the evaluation of the creep damage during the tensile strain holding. Based on the results obtained the following conclusions are drawn:

(1) The fatigue life reduction due to the strain holding is observed even at hold times of 6 seconds, and the saturation point of the fatigue life reduction shifts to the shorter hold time side with increasing temperature.

(2) The life fraction rule predicts an excessively conservative value for the creep damage.

(3) The ductility exhaustion rule can predict the fatigue life under the effective creep condition much more successfully than the life fraction one.

Acknowledgments

The authors are grateful to Dr. T. Kondo of the Japan Atomic Energy Research Institute (JAERI) for his advice and encouragement. The authors also greatly appreciate the assistance in data handling calculation by Mr. S. Kita, a visiting technician to the JAERI.

4. Conclusions

The properties of Hastelloy XR under creep-fatigue interaction conditions were examined by performing a series of axial strain controlled fully reversed fatigue tests in the simulated HTGR helium gas environment at 700, 800, 900 and 950°C. Two types of evaluation techniques, i.e., the life fraction rule and the ductility exhaustion one, were applied for the evaluation of the creep damage during the tensile strain holding. Based on the results obtained the following conclusions are drawn:

(1) The fatigue life reduction due to the strain holding is observed even at hold times of 6 seconds, and the saturation point of the fatigue life reduction shifts to the shorter hold time side with increasing temperature.

(2) The life fraction rule predicts an excessively conservative value for the creep damage.

(3) The ductility exhaustion rule can predict the fatigue life under the effective creep condition much more successfully than the life fraction one.

Acknowledgments

The authors are grateful to Dr. T. Kondo of the Japan Atomic Energy Research Institute (JAERI) for his advice and encouragement. The authors also greatly appreciate the assistance in data handling calculation by Mr. S. Kita, a visiting technician to the JAERI.

REFERENCES

[1] K. Hada, I. Nishiguchi, Y. Muto and H. Tsuji, Nucl. Eng. Des. 132 (1991) 1.

[2] Japan Atomic Energy Research Institute, Present Status of HTGR Research & Development (1992).

[3] M. Shindo and T. Kondo, in: Proc. Conf. on Gas-Cooled Reactors Today, Bristol/UK, 1982 (British Nuclear Energy Society) Vol.2, p.179.

[4] E.L. Robinson, Trans. ASME 60 (1938) 253.

[5] E.L. Robinson, Trans. ASME 74 (1952) 777.

[6] H.G. Edmunds and D.J. White, J. Mech. Eng. Sci. 8-3 (1966) 310.

[7] R.H. Priest and E.G. Ellison, Mat. Sci. and Eng. 49 (1981) 7.

[8] R. Hales, Fat. Energ. Mater. Struct. 6 (1983) 121.

[9] M. Okada, T. Tanabe, F. Abe, Y. Sakai, T. Kondo, H. Nakajima, Y. Ogawa, H. Tsuji and Y. Kurata, Creep and Fatigue Behaviors of Some Ni-Cr-W Superalloys for High-Temperature Gas-Cooled Reactors in Simulated Helium Environments, Japan Atomic Energy Research Institute, Research Report JAERI-M 87-193 (November 1987).

[10] H. Tsuji and T. Kondo, J. Nucl. Mater. 150 (1987) 259.

[11] H. Tsuji and T. Kondo, Time-Dependent High-Temperature Low-Cycle Fatigue Behavior of Nickel-Base Heat-Resistant Alloys for HTGR, Japan Atomic Energy Research Institute, Research Report JAERI-M 88-099 (June 1988).

[12] Japanese Industrial Standards Committee, Method of High Temperature Low Cycle Fatigue Testing for Metallic Materials (JIS Z 2279) (Japanese Standards Association, 1992).

[13] H. Tsuji, T. Tanabe, Y. Nakasone and H. Nakajima, J. Nucl. Mater. 199 (1992) 43.

[14] H. Tsuji, T. Tanabe, Y. Nakasone and H. Nakajima, J. Nucl. Sci. Technol. 30 (1993) 768.

[15] F.R. Larson and J. Miller, Trans. ASME 74 (1952) 765.

[16] M.A. Miner, J. Appl. Mech., 12-3 (1945) A159.

[17] S. Taira, Creep in Structures ed. by N.J. Hoff (Academic Press, New York, 1962) p.96.

Table 1 Chemical composition of the material tested (unit: mass%).

	C	Si	Mn	P	S	Cr	Co	Mo	W	Fe	B	Al	Ti	N	Ni
T	0.07	0.32	0.96	<0.001	<0.001	22.00	0.02	9.11	0.49	18.59	0.0002	0.01	0.01	0.007	Bal.
B	0.07	0.33	0.93	<0.001	<0.001	21.96	0.03	9.11	0.49	18.62	0.0001	0.02	<0.01	0.006	Bal.

T : Top side of the ingot, B : Bottom side of the ingot

Table 3 Impurity levels in simulated HTGR helium gas environment (unit: vol ppm).

Impurity	H_2	H_2O	CO	CO_2	CH_4
Nominal value	200	1	100	2	5
Analyzed value	190 to 210	0.8 to 1.2	90 to 110	1.5 to 2.5	4 to 6

Table 2 Tensile properties of the material tested at room temperature and at high temperatures.

Test Temp.	Strain Rate	0.2% Proof Stress	Ultimate Tensile Strength	Total Elongation	Reduction of Area
RT	5×10^{-3} %/s (first stage) 1.25×10^{-1} %/s (second stage) Strain rate was changed at a strain of 1.5 %.	301 to 323 MPa	688 to 697 MPa Frequency was four.	57.1 to 62.8 %	62.8 to 64.6 %
700℃	5×10^{-3} %/s	187 MPa	450 MPa	67.4 %	58.4 %
	1.25×10^{-1} %/s	169 MPa	419 MPa	57.2 %	55.0 %
	2.5×10^{-1} %/s	149 MPa	417 MPa	59.6 %	57.6 %
800℃	5×10^{-3} %/s	156 MPa	206 MPa	83.0 %	74.0 %
	1.25×10^{-1} %/s	158 MPa	312 MPa	79.2 %	72.3 %
	2.5×10^{-1} %/s	153 MPa	331 MPa	67.6 %	67.2 %
850℃	5×10^{-3} %/s	188 MPa	203 MPa	116.3 %	75.2 %
	1.25×10^{-1} %/s	155 MPa	250 MPa	108.9 %	80.2 %
	2.5×10^{-1} %/s	147 MPa	274 MPa	84.6 %	74.3 %
900℃	5×10^{-3} %/s	153 MPa	172 MPa	126.2 %	69.2 %
	1.25×10^{-1} %/s	149 MPa	195 MPa	101.1 %	82.5 %
	2.5×10^{-1} %/s	146 MPa	217 MPa	101.5 %	78.5 %
950℃	5×10^{-3} %/s	117 MPa	137 MPa	94.6 %	67.2 %
	1.25×10^{-1} %/s	136 MPa	172 MPa	122.3 %	83.8 %
	2.5×10^{-1} %/s	143 MPa	171 MPa	101.7 %	80.7 %
1000℃	5×10^{-3} %/s	81 MPa	103 MPa	86.7 %	64.1 %
	1.25×10^{-1} %/s	123 MPa	136 MPa	132.7 %	84.0 %
	2.5×10^{-1} %/s	129 MPa	145 MPa	100.4 %	79.6 %

Table 4 Results of low-cycle fatigue tests with symmetric strain waveform.

Test temp. (℃)	Total strain range (%)	Elastic strain range at $\frac{1}{2}N_f$ (%)	Inelastic strain range at $\frac{1}{2}N_f$ (%)	Number of cycles to failure
700	0.40	0.33	0.07	32971
	0.80	0.43 (0.434944)	0.36 (0.361994)	2011
	0.80	0.46 (0.456999)	0.34 (0.340115)	1717
	1.20	0.54	0.66	647
800	1.20	0.37	0.83	799
	0.40	0.26	0.14	12897
	0.80	0.32	0.48	1670
900	0.40	0.22	0.18	5713
	0.80	0.22	0.58	1103
	1.20	0.24	0.96	497
950	0.40	0.19	0.21	5195
	0.80	0.20 (0.203634)	0.59 (0.59332)	1147
	1.20	0.21	0.99	453

Table 5 Results of low-cycle fatigue tests with trapezoidal strain waveform.

Test temperature (℃)	Total strain range (%)	Hold time (s)	Number of cycles to failure
700	0.40	60	7759
	0.80	60	1505
			1285
		600	713
		3600	312
800	0.40	60	2411
	0.80	6	1123
		60	447
		600	384
		3600	291
900	0.40	60	1468
	0.80	6	870
		60	562
		600	432
950	0.40	60	1613
	0.80	6	872
		60	607
		600	335

Table 6 Results of damage evaluation.

Test temp. (℃)	Total strain range (%)	Hold time (s)	D_{cl}/cycle at 1/2 N_f (during strain holding)	D_{cl}	D_{cd}/cycle at 1/2 N_f (during strain holding)	D_{cd}	D_f/cycle	D_f
700	0.40	60	5.68216×10^{-4}	4.41	9.1308×10^{-5}	0.71	3.3641×10^{-5}	0.26
	0.80	60	2.752822×10^{-3}	4.14	5.2953×10^{-4}	0.80	5.1361×10^{-4}	0.77
		60	4.39548×10^{-3}	5.65	8.8006×10^{-4}	1.13	5.1361×10^{-4}	0.66
		600	4.807956×10^{-3}	3.43	8.5869×10^{-4}	0.61	5.1361×10^{-4}	0.37
		3600	4.790423×10^{-3}	1.49	8.4082×10^{-4}	0.26	5.1361×10^{-4}	0.16
800	0.40	60	9.03406×10^{-4}	2.18	3.0166×10^{-4}	0.73	8.1070×10^{-5}	0.20
	0.80	6	1.75925×10^{-3}	1.98	7.250×10^{-4}	0.81	5.5036×10^{-4}	0.62
		60	5.0119×10^{-3}	2.24	1.9802×10^{-3}	0.89	5.5036×10^{-4}	0.25
		600	3.21273×10^{-3}	1.23	1.2093×10^{-3}	0.46	5.5036×10^{-4}	0.21
		3600	2.48277×10^{-3}	0.72	8.995×10^{-4}	0.26	5.5036×10^{-4}	0.16
900	0.40	60	9.2025×10^{-4}	1.35	4.9653×10^{-4}	0.73	1.7565×10^{-4}	0.26
	0.80	6	1.25795×10^{-3}	1.09	7.138×10^{-4}	0.62	9.2421×10^{-4}	0.80
		60	1.61575×10^{-3}	0.91	8.9×10^{-4}	0.50	9.2421×10^{-4}	0.52
		600	1.51214×10^{-3}	0.65	8.026×10^{-4}	0.35	9.2421×10^{-4}	0.40
950	0.40	60	6.5546×10^{-4}	1.06	7.681×10^{-4}	1.24	1.8454×10^{-4}	0.30
	0.80	6	8.2012×10^{-4}	0.72	5.76×10^{-4}	0.50	9.5329×10^{-4}	0.83
		60	1.0931×10^{-3}	0.66	7.451×10^{-4}	0.45	9.5329×10^{-4}	0.58
		600	1.25774×10^{-3}	0.42	1.4086×10^{-3}	0.47	9.5329×10^{-4}	0.32

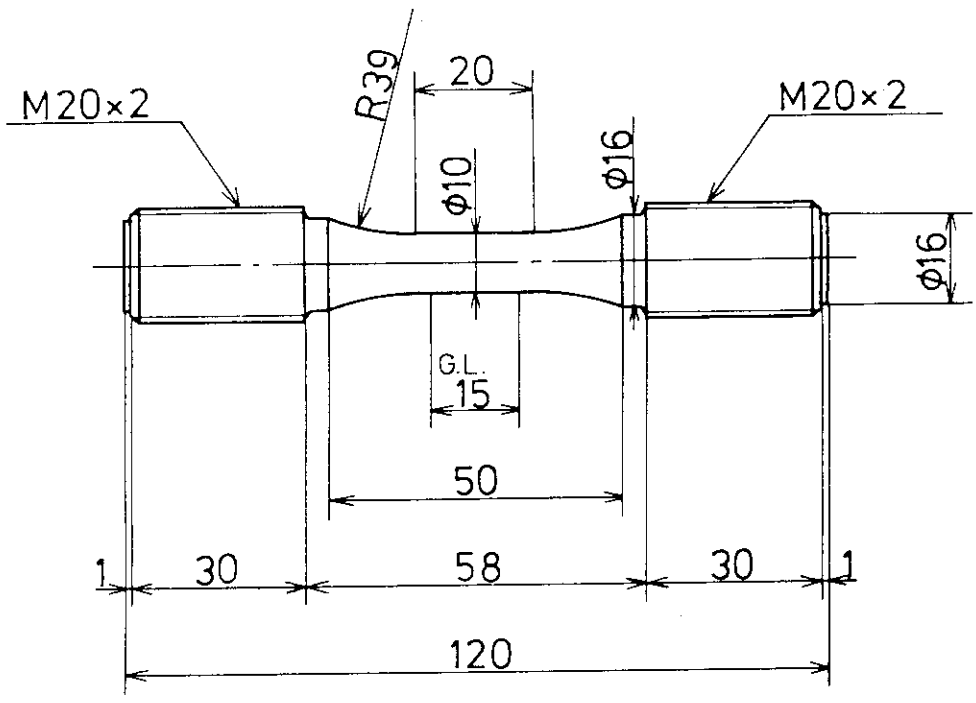

Fig. 1 Geometry of the specimen (unit: mm).

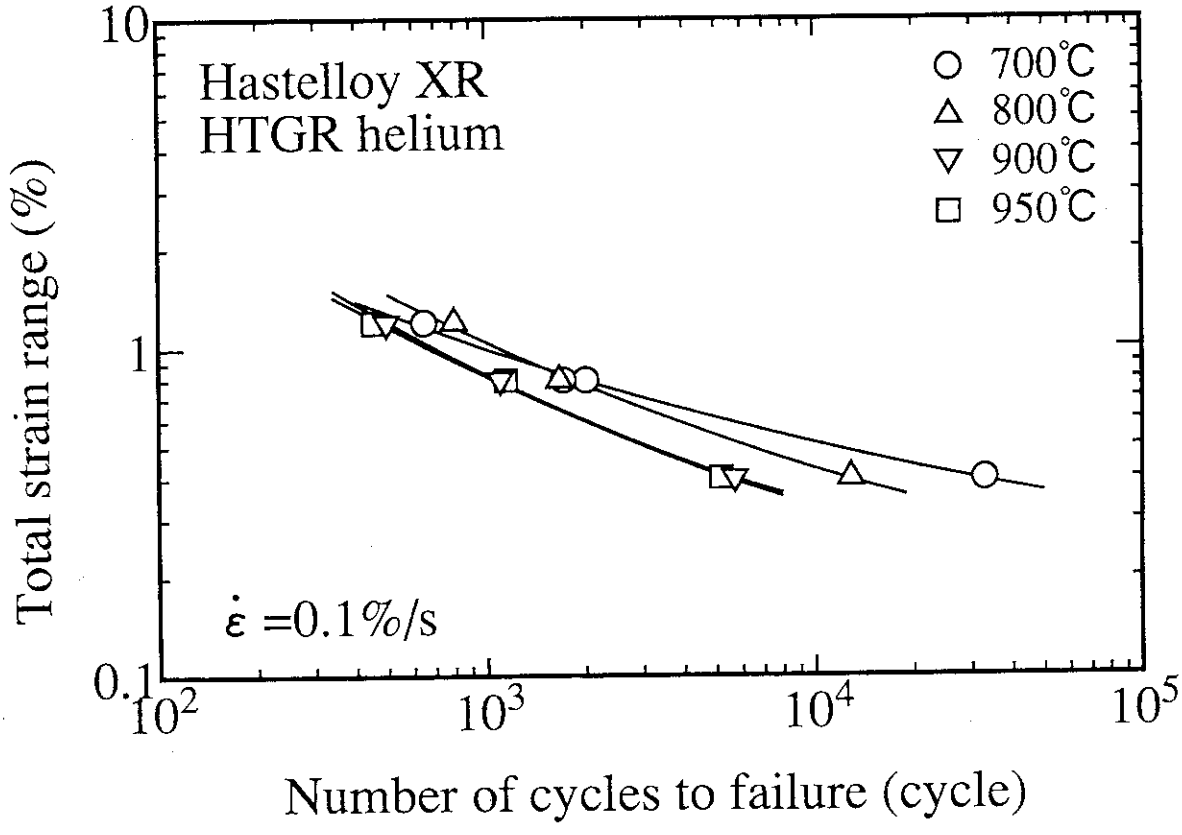

Fig. 2 Relation between the total strain range and the number of cycles to failure obtained with the symmetric triangular waveform.

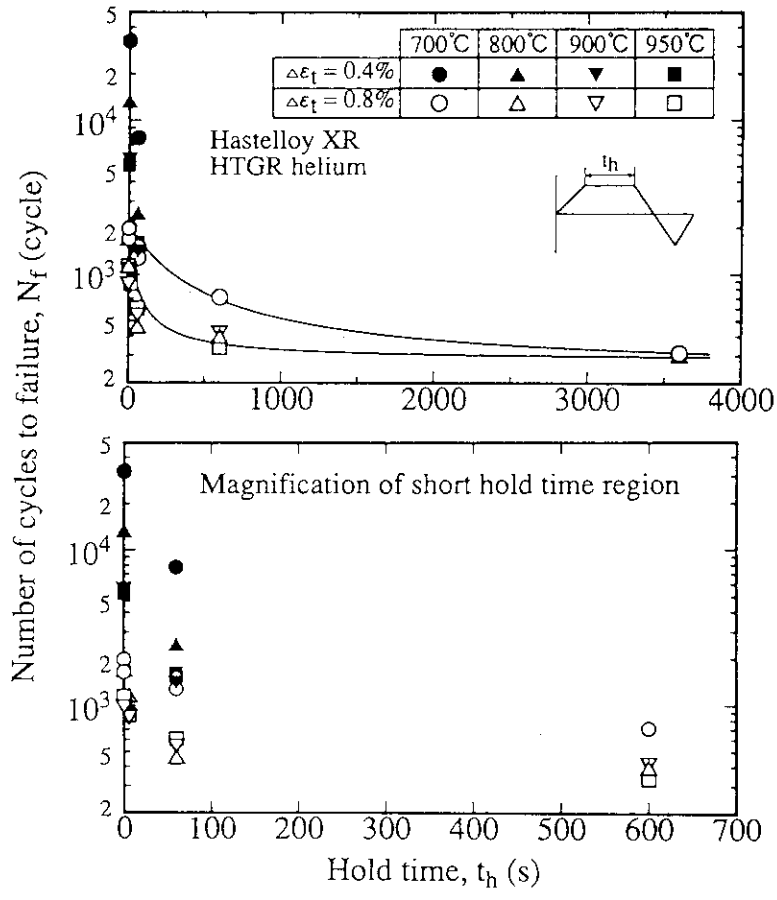

Fig. 3 Relation between the fatigue life and the strain hold time obtained with the trapezoidal waveform.

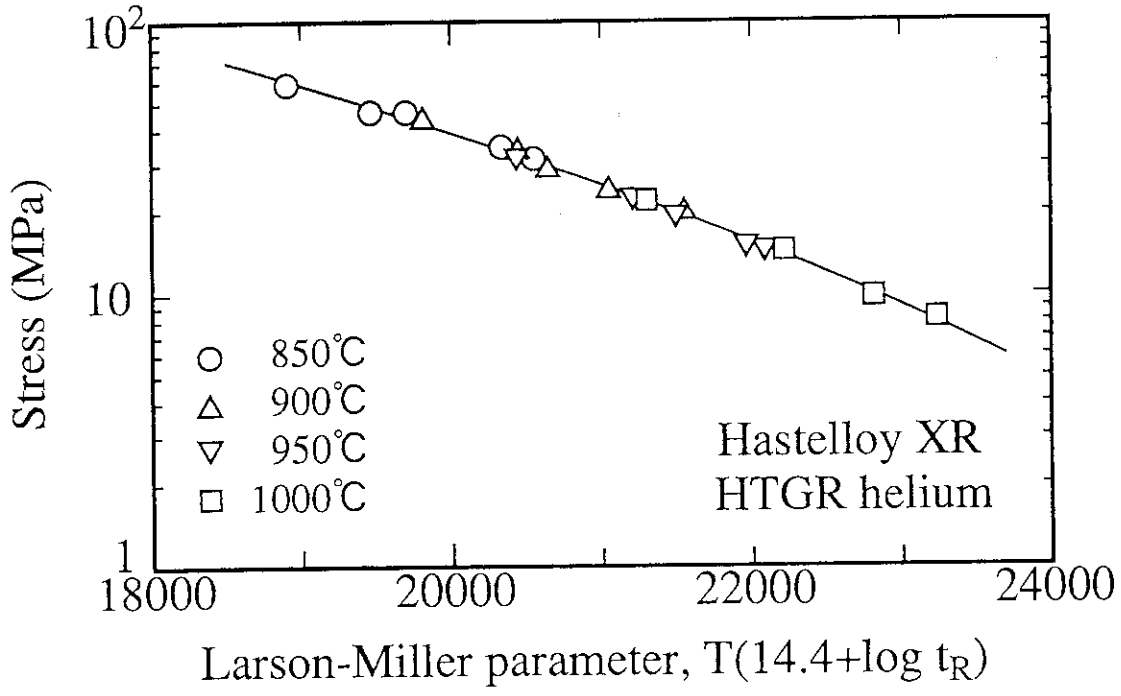

Fig. 4 Relation between the applied stress and the Larson-Miller parameter, where "T" is the temperature in Kelvin and t_R is the time to rupture in hour. The data originated from other studies by the authors [13,14] for the same heat material as that in the present study.

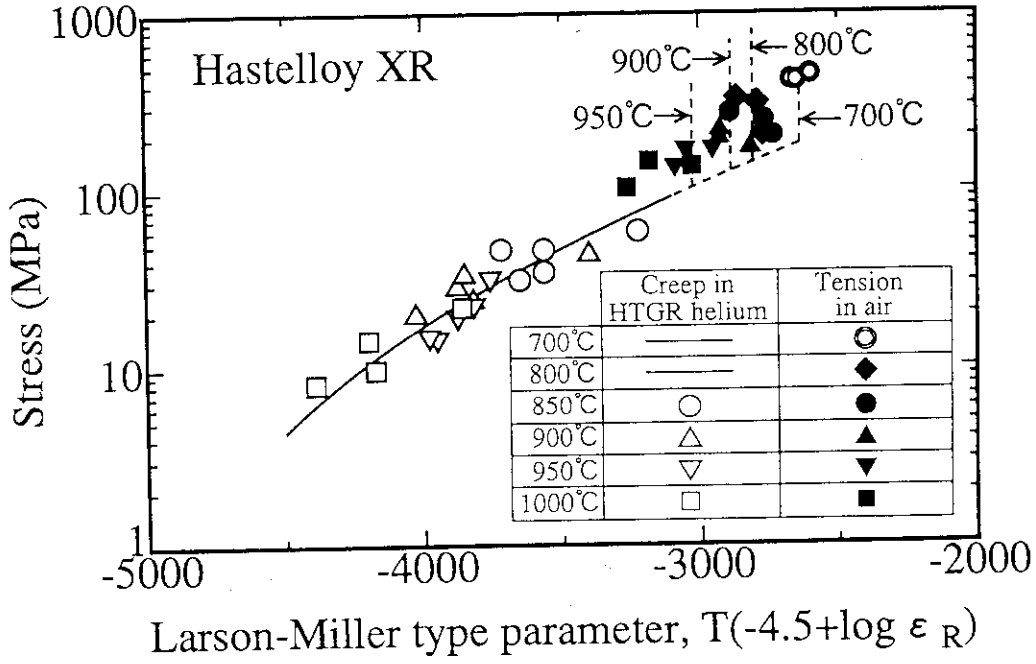

Fig. 5 Relation between the stress and the Larson-Miller type parameter concerning the strain at rupture, where "T" is the temperature in Kelvin and ε_R is the strain at rupture in percent. The creep data originated from other studies by the authors [13,14] for the same heat material as that in the present study.

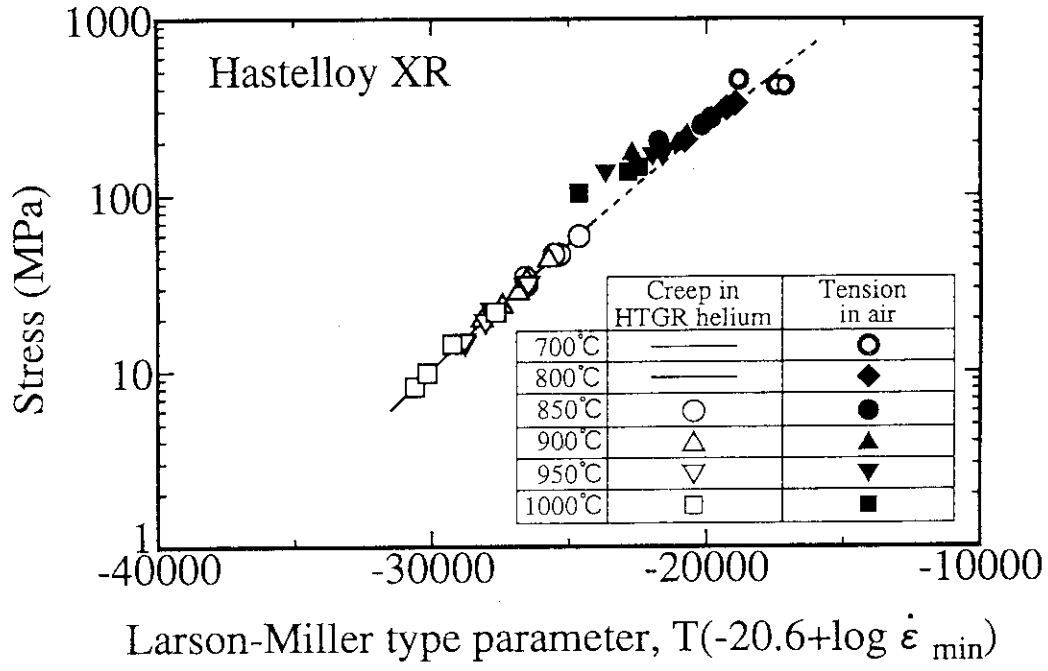

Fig. 6 Relation between the stress and the Larson-Miller type parameter concerning the minimum creep rate, where "T" is the temperature in Kelvin and $\dot{\varepsilon}_{min}$ is the minimum creep rate or the strain rate for creep or tensile data, respectively, in %/h. The creep data originated from other studies by the authors [13,14] for the same heat material as that in the present study.

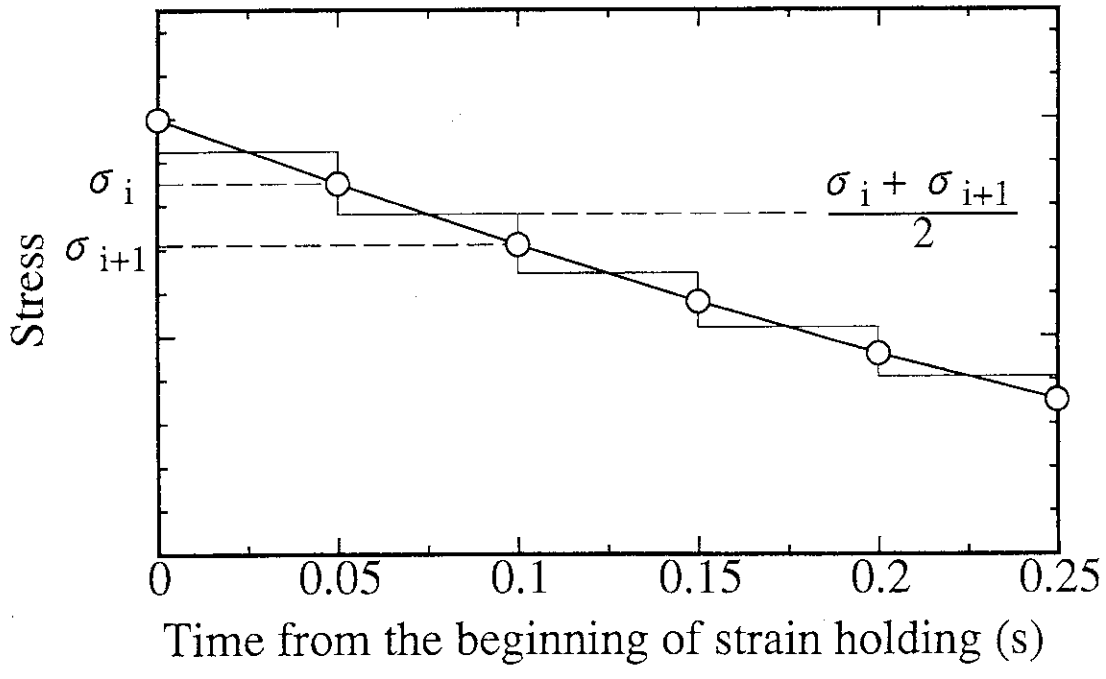

Fig. 7 Schematic illustration of the determination method of the stress level used for the creep damage evaluation during the strain holding.

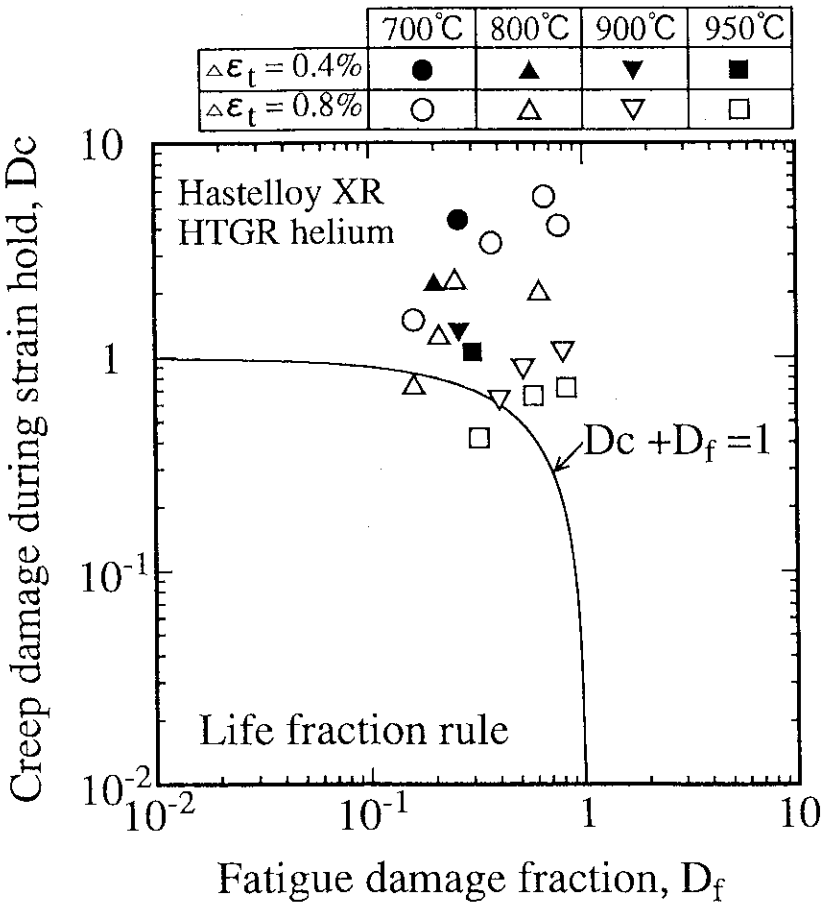

Fig. 8 Fatigue damage versus creep damage plots. Creep damage was evaluated by the life fraction rule.

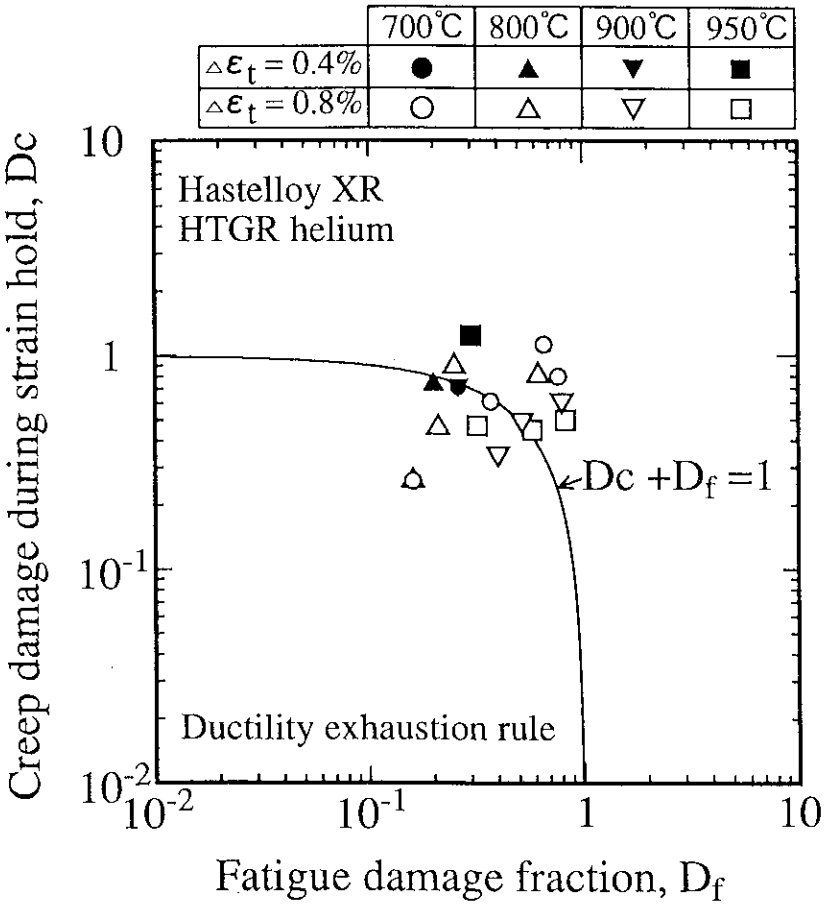

Fig. 9 Fatigue damage versus creep damage plots. Creep damage was evaluated by the ductility exhaustion rule.

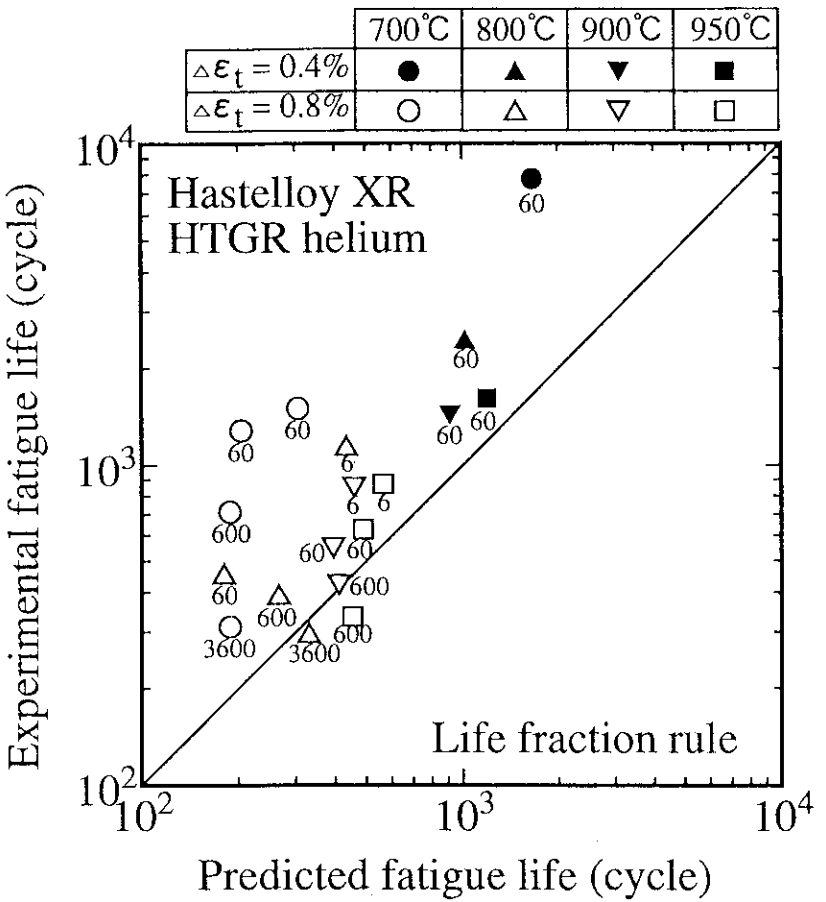

Fig. 10 Relation between the experimental and the predicted fatigue lives by the life fraction rule. Figures indicate the strain hold time in seconds.

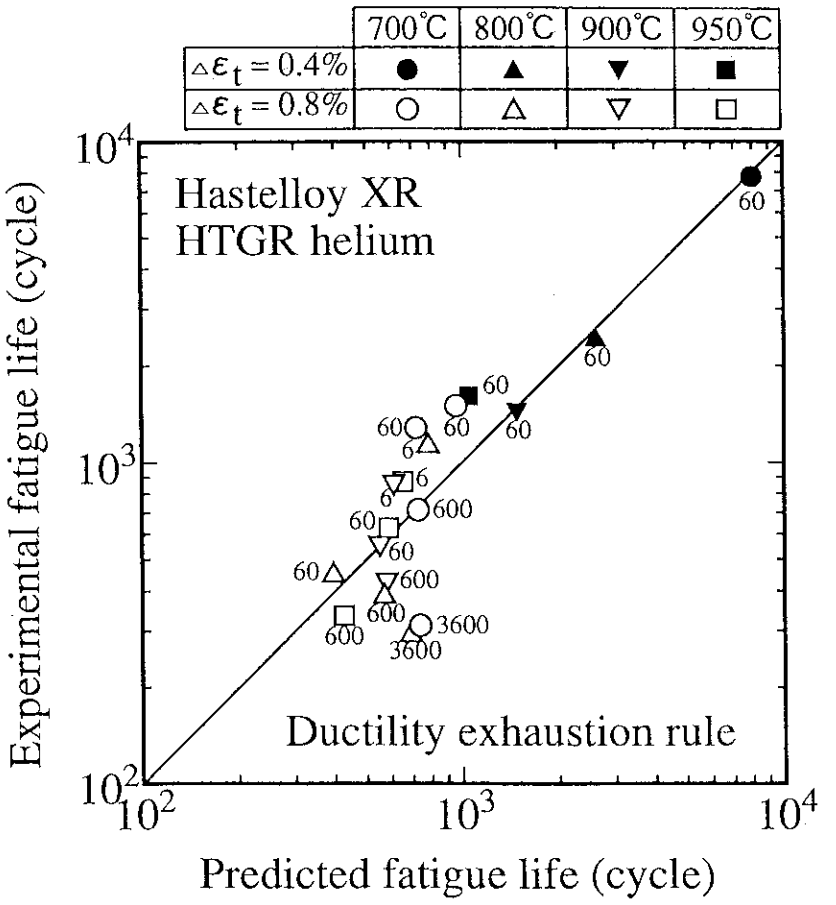

Fig. 11 Relation between the experimental and the predicted fatigue lives by the ductility exhaustion rule. Figures indicate the strain hold time in seconds.